Dale P. Bentz[1] and Paul E. Stutzman[1]

# SEM ANALYSIS AND COMPUTER MODELLING OF HYDRATION OF PORTLAND CEMENT PARTICLES

**REFERENCE:** Bentz, D. P. and Stutzman, P. E., **"SEM Analysis and Computer Modelling of Hydration of Portland Cement Particles,"** Petrography of Cementitious Materials, ASTM STP 1215, Sharon M. DeHayes and David Stark, Eds., American Society for Testing and Materials, Philadelphia, 1994.

**ABSTRACT:** Characterization of cement particles is complicated due to their wide size range, complex shapes, and multi-phase nature. Accurate characterization should allow for better prediction of cement performance and more realistic modelling of cement microstructural development. This paper presents a technique, based on scanning electron microscopy and digital image processing, for obtaining two-dimensional digital images of actual portland cement particles in which all major phases are identified. By combining backscattered electron and X-ray images, an image segmented into the major cement phases may be created. These images can be analyzed to determine any number of quantitative measures such as phase fractions or phase perimeters. The technique has also been successfully utilized in obtaining realistic starting images for input into a two-dimensional cement microstructure model which simulates the hydration process.

**KEYWORDS:** building technology, cement particles, characterization, hydration, image processing, interfacial zone, microstructure, phase analysis, scanning electron microscopy, simulation, X-ray images.

The processes by which cement paste transforms from a viscous suspension into a rigid solid must be understood if the performance of concrete and other cement-based materials is to be reliably predicted from the properties of their constituents. While the hydration reactions and mechanisms have not been completely elucidated, the topic is further complicated by a lack of a quantitative description of the anhydrous cement particles. Both the bulk composition of a cement and the spatial distribution of the various phases will influence the temporal properties of a hydrating system. Quantification of the initial cement particles is thus seen as an important step in developing scientifically-based relationships between cement microstructure and resultant properties such as strength and durability. Additionally, such quantification could serve as a valuable quality control technique for the cement production industry, ultimately leading to a new

[1] Chemical engineer and physical scientist respectively, Building Materials Division, Building and Fire Research Laboratory, National Institute of Standards and Technology, U.S. Department of Commerce, Gaithersburg, MD 20899.

generation of cement and concrete standards.

In recent years, the application of scanning electron microscopy (SEM) to characterizing cement clinker and ground cements has increased. SEM and X-ray microanalysis have been utilized to identify the four major phases in portland cement clinker [1]. Scrivener has applied similar techniques to determine the distribution of silicates and interstitial phases in cement grains [2] and compared the results to the rates of heat release during hydration. Bonen and Diamond have analyzed the same cement clinker ground in both a ball mill and a high pressure roller mill, using SEM and X-ray analysis to classify the predominant phase found in each cement particle [3]. Additionally, the particles were characterized on the basis of aspect ratio and shape factor using image analysis techniques.

Another recent development in the field of cement research is the use of computer modelling to relate microstructure to properties. Often, these models are digital-image-based, with a two or three-dimensional digital image being the basis for the microstructure model [4]. The underlying image structure allows for the efficient computation of properties such as ionic diffusivity or elastic modulus [5]. While simplifications such as using circular particles can be made, these models can accept actual images of cement particles as input. It was therefore of interest to develop techniques to obtain images of cement particles in which each pixel (element) in the image has been classified as a phase of portland cement. This paper details the technique developed to obtain two-dimensional images of the real anhydrous cement particles and provides examples of using these images as input into a computer model of the microstructural development of hydrating cement paste.

## EXPERIMENTAL METHOD

### Sample Preparation

Proper sample preparation is critical to the successful imaging of fine cement particles. Difficulties encountered in preparing polished sections of cement include the elimination of scratches, edge rounding, surface relief, and grain plucking.

To prepare a specimen for viewing in the SEM, about 25 grams of the cement powder of interest are blended with an epoxy resin[2] to form an almost dry paste. The epoxy resin has a viscosity close to that of water so that this specimen will be similar to a suspension of cement particles in water. The paste is pressed into a sample mold and cured at 60 °C for 24 hours. The cured specimen is cut using a low-speed diamond wafering saw, cutting first a layer from the outer surface and then about 10 mm into the sample. This two-cut procedure produces parallel faces, minimizing the need to refocus as one traverses a specimen.

Saw marks are easily removed by dry grinding with 400 grit followed by 600 grit sandpaper. Final polishing is done on a lap wheel with 6, 3, 1, and 0.25 μm diamond paste for about 30 seconds each. We have been able to produce low relief, fine polishes using a lint-free

---

[2] EpoTek 301, Epoxy Technology Corporation, Billerica, Mass. This and other tradenames and company products are identified to adequately specify the experimental procedure. In no case does such identification imply recommendation or endorsement by the National Institute of Standards and Technology, nor does it imply that the products are necessarily the best available for the purpose.

polyester SEM cleaning cloth[3] and diamond paste on top of Texmet paper. The specimen is cleaned after each polishing stage by gently wiping on a clean cloth; residual polishing compound is removed with ethanol after the final polishing stage. Repeated cleaning with ethanol is avoided because it may soften the epoxy and increase the chance of grain plucking. The specimen is then coated with carbon to provide a conductive surface for viewing in the SEM.

## SEM Imaging

When viewed in the SEM, signals emitted from the sample as a result of the specimen-primary electron beam interaction include backscattered electrons (BE) and X-rays. For this study, an accelerating voltage of 12 kV and probe current of about 2 nA was used for collecting the BE images, while probe currents of about 10 nA were used for X-ray imaging.

In the BE images, brightness is proportional to the average atomic number ($\bar{Z}$) of a phase. For the major phases present in portland cement, the phases from brightest to darkest are tetracalcium aluminoferrite ($C_4AF$), tricalcium silicate ($C_3S$), tricalcium aluminate ($C_3A$) and dicalcium silicate ($C_2S$), gypsum, and the resin-filled voids. Because the BE signal is weak, BE images are inherently noisy so that often the noise is reduced by averaging images of the same field of view. Phase identification can then be attempted by segmenting the BE image based on analysis of the greylevel histogram (a histogram of the number of pixels in the image assigned to each greylevel or intensity). While some phase segmentation is possible, a completely accurate separation cannot be based solely on the BE image since several of the phases (such as $C_3A$ and $C_2S$) have similar intensities ($\bar{Z}$ values) even though they differ widely in chemical composition.

To supplement the information content of the BE image, X-ray images are obtained for the elements calcium, iron, aluminum, and sulfur. A typical X-ray spectrum from an energy dispersive X-ray detector appears in Figure 1 as a plot of signal intensity vs energy level. X-ray images are created by slowly scanning the specimen while measuring X-ray counts within energy windows encompassing a peak for the element of interest. Typically, about three hours of scan time is required to obtain a set of 512*400 X-ray images. These images of X-ray signal intensity can be processed and analyzed in the same manner as the BE image, and can even be combined with the BE image.

## Image Processing

Figure 2 shows the BE image and the four X-ray images for an ASTM Type I portland cement. In these images, each pixel is about 0.5 $\mu$m on a side, which is near the resolution limit for X-ray images. For the iron, aluminum, and sulfur X-ray images, the threshold levels used to produce binary images were determined by finding a local minimum in the greylevel histogram for each image. For calcium, the X-ray image is segmented into four levels, indicating high, medium, low, and no calcium content, depending on the local (pixel) intensity of the X-ray signal. By combining these four X-ray images with the BE image, each of the four main clinker phases of a portland cement along with gypsum may be distinguished. For instance, the presence of iron in the X-ray image indicates the tetracalcium aluminoferrite phase while the presence of aluminum but not iron indicates the tricalcium aluminate phase. Similarly, gypsum is indicated by the presence of sulfur. Here, we should note that all sulfates, including the sodium and potassium sulfates, are assigned to be gypsum, since the microstructure model

---

[3] Lint-free cleaning cloths are available from most SEM suppliers.

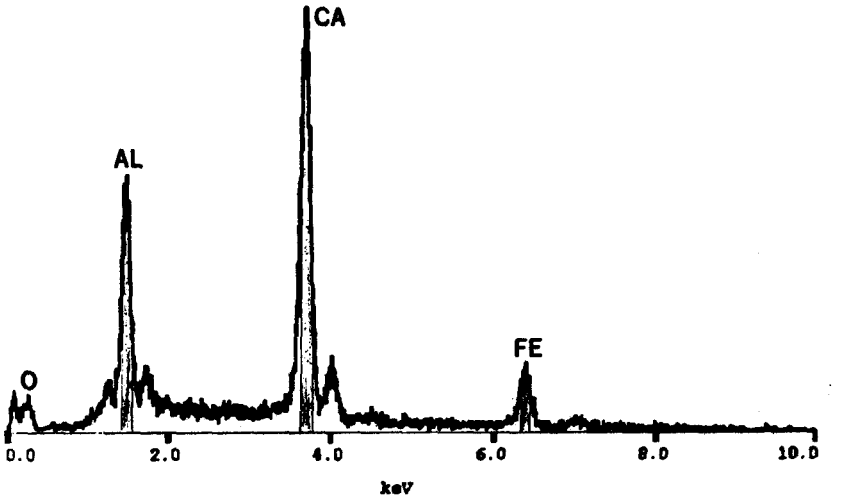


Figure 1. X-ray spectrum of tetracalcium aluminoferrite indicating a composition of calcium (Ca), iron (Fe), aluminum (Al), and oxygen (O). The vertical bars indicate the peak window region used for generating an X-ray image.

described later assumes all sulfates will react with aluminates to form ettringite and monosulfoaluminate. If further segmentation were required, however, the X-ray images for sodium and potassium could be used to distinguish the various alkali sulfates from gypsum. Finally, the tricalcium and dicalcium silicate are identified based on the intensity of the BE and calcium X-ray images, where the brighter areas in these images correspond to the tricalcium silicate phases. If the calcium X-ray and BE images are insufficient to separate the silicate phases, an X-ray image for silicon is collected to process along with these two images. Here, segmentation can be based on the calcium/silicon ratio, which should be higher for $C_3S$ than for $C_2S$.

The segmented image produced in this fashion still contains noise and some pixels which are not porosity but which have not been assigned to one of the solid phases. To sharpen the phase distinction and eliminate the noise, the image is filtered using a median filter. Here, each "solid" pixel in the image is reassigned to be the phase occupied by the majority of its neighbors, excluding (resin-filled) porosity, if this majority exceeds a preset limit. Applying these processing steps to the images in Figure 2 results in the final image shown in Figure 3. The complexity of both shape and phase distribution for the cement particles shown in Figure 3 suggests that the artificial computer generation of such particles would be a formidable task, reinforcing the importance of the experimental technique described herein.

Images like those shown in Figure 3 can be further processed in a number of ways. The shapes and phase distributions of the individual cement particles can be stored in a database using a line segment encoding technique [6] and used to create computer-assembled images representing a given cement at a variety of water-to-cement (w/c) ratios, where the porosity is now assumed to be filled with water. The areas of the individual cement particles also can be assessed, although converting this two-dimensional size distribution to a true three-dimensional particle size distribution is possible only when assumptions

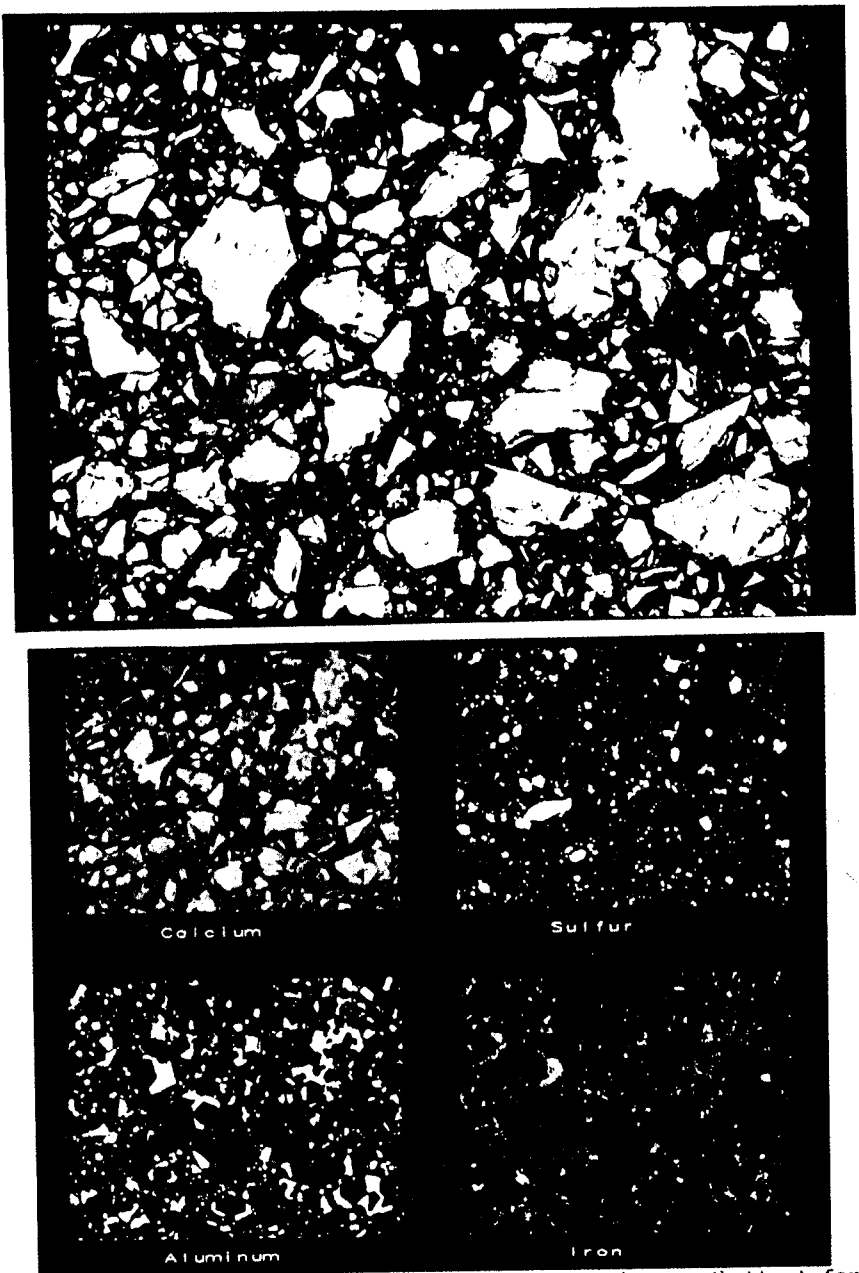


Figure 2. Backscattered electron (top) and X-ray images (bottom) for a real Type I portland cement.


Figure 3. Final 256*199 μm (512*398 pixel) image of real cement particle microstructure (w/c=0.36) for images shown in Figure 2. Phase colors are as indicated in color bars at the bottom of the image.

concerning particle geometry (such as assuming spherical particles) are made [7]. The bulk area fractions, which should correspond to volume fractions [7], can be computed by simply counting the number of pixels assigned to each phase. These fractions can then be compared to those computed on a volume basis by applying the Bogue calculation to the oxide composition of the cement. Since cement hydration is critically dependent on the contact surface between water and the cement particles, the perimeter or surface fraction of each of the phases is also a quantity of interest. This measure can be determined by counting those pixel edges separating porosity and solid pixels for each solid phase.

## CEMENT HYDRATION MICROSTRUCTURE MODEL

At the National Institute of Standards and Technology (NIST), images such as the one in Figure 3 have been used extensively as input to a digital-image-based cement hydration microstructure model. The goal of the model is to simulate the microstructure of cement paste as it hydrates. Hydrated microstructures are then numerically evaluated to compute physical properties such as ionic diffusivity or elastic modulus, to quantitatively relate microstructure to properties and design improved materials [4]. Initially, the microstructure model was based solely on the hydration of $C_3S$, the major component of portland cement, but it recently has been extended to include hydration reactions for all of the major phases [8].

The model is based on a cyclic process of dissolution, diffusion, and reaction, and is similar to a cellular automaton [8]. Basically, material dissolves in pixel-sized units from the cement particle surfaces, diffuses within the water-filled pore space, and reacts to form hydration products. The silicate phases form calcium silicate hydrate (C-S-H) gel and calcium hydroxide (CH) while the interstitial (aluminate and ferrite) phases form a variety of products (hydrogarnet- $C_3AH_6$, ettringite- AFt, and a monosulfoaluminate phase- AFm) depending on the amount of gypsum present in the system. Both surface-precipitated products such as the C-S-H gel and crystalline products such as CH are included in the rules representing the physical mechanisms of cement hydration. Both the chemical (molar) stoichiometry of the reactions that occur during hydration and the molar volumes of the products and reactants determine the volume (pixel) stoichiometry implemented within the digital-image-based computer model. For example, for each pixel of $C_3S$ which dissolves, 1.75 pixels of C-S-H gel and 0.61 pixels of CH will be formed. Since the hydration products occupy a larger volume than the solid reactants, the cement paste ultimately converts from a viscous suspension into a rigid solid material.

It is well known that the various phases of cement react at different rates in a cement paste. Within the model, probabilities can be assigned to the dissolution processes so that the rank order of these phase reactivities can be maintained (e.g. $C_3A > C_3S > C_2S$, $C_4AF$). The mobility of various diffusing species may be controlled by choosing the location of a diffusing species relative to the location of the dissolution source. Silicate and iron diffusing species are located near the dissolution source to simulate their low mobility, while calcium, sulfate, and aluminate species are located at random throughout the microstructure, representing a uniform dispersion of these species. By monitoring the reactions occurring in a given cycle of hydration, the heat of hydration as a function of the number of cycles or the degree of hydration may be obtained. For this calculation, either the heats of formation of the cement compounds or tabulated values of the heats of hydration of the four main cement phases may be used [9,10].

Once cement particles have been stored in a database, they may be utilized to study the formation of interfacial zone microstructure. Interfacial zones in concrete have been shown to exhibit different microstructural characteristics than bulk cement paste both for cement paste-aggregate [11,12] and cement paste-steel rebar [13] interfaces. A simpler version of the NIST microstructure model has been successfully applied to simulating interfacial zone microstructures as a function of mineral admixture characteristics and aggregate absorptivity and reactivity [14]. For this model, a simple two-dimensional rectangular aggregate is first placed into the microstructure image and then the stored cement particles are added at random locations in the microstructure to obtain a representation of the desired global w/c ratio. The cement particles are not allowed to overlap any previously placed particle or any portion of the aggregate and are added in order of largest to smallest. The interfacial zone microstructure may be quantified by measuring the phase fractions as a function of distance from the aggregate surface both before and after hydration. These measurements may then be compared to those obtained from SEM images of real concrete specimens [14].

## RESULTS

### Area Fractions and Phase Perimeters

Table 1 shows the area and perimeter phase fractions for two different fields of view for the cement shown in Figure 3. It should be noted that the perimeter fractions will be a stronger function of image

resolution than the area fractions. In both cases, the bulk area fractions are quite similar to the volume fractions computed using the Bogue equations [9]. Since most of the larger silicate particles are $C_3S$, the $C_3S$ particles generally have a lower surface area to volume (or perimeter to area) ratio than the $C_2S$ particles. Thus, the $C_2S$ occupies a larger fraction of the phase perimeters than its area fraction. The $C_2S$ generally reacts at a slower rate than the $C_3S$ suggesting that this cement might hydrate at a slower rate than a cement with the same bulk phase fractions but a proportional distribution of the two silicates on its surfaces. Since the gypsum is generally present as smaller discrete particles, it too occupies a larger perimeter fraction than its area fraction.

Scrivener has computed the area and surface fractions of silicates and interstitial phases and in general found that the interstitial phases occupied a larger fraction of the surfaces than their area fraction [2]. For this particular cement, we actually observe the opposite trend, as the interstitial phases (ferrite and aluminate) occupy a smaller perimeter fraction than their area fraction. This can be directly observed in Figure 3, where many of the $C_3A$ regions are part of much larger polymineralic particles and have much of their perimeter in contact with $C_3S$ instead of porosity.

Table 1
Area and Perimeter Phase Fractions for a Type I Portland Cement

| | | Image 1 | | Image 2 | |
|---|---|---|---|---|---|
| | Bogue Volume Fraction | Area Fraction | Perimeter Fraction | Area Fraction | Perimeter Fraction |
| $C_3S$ | 0.618 | 0.637 | 0.397 | 0.648 | 0.445 |
| $C_2S$ | 0.127 | 0.115 | 0.322 | 0.121 | 0.316 |
| $C_3A$ | 0.145 | 0.177 | 0.157 | 0.144 | 0.124 |
| $C_4AF$ | 0.058 | 0.018 | 0.013 | 0.044 | 0.021 |
| Gypsum | 0.051 | 0.053 | 0.111 | 0.043 | 0.093 |

## Heat of Hydration Results

Figure 4 shows two different initial cement particle images, both at a w/c of 0.45. The area and perimeter fractions for these two cement images are provided in Table 2. In Figure 5, calculated heat of hydration is plotted versus calculated degree of hydration for results obtained using the microstructure model to hydrate each cement for 200 cycles. As expected, a basically linear relationship is observed between heat evolved and degree of hydration. Since the two cements differ in bulk and surface compositions as shown in Table 2, their heat release characteristics also vary. Because Cement 1 has a higher $C_3A$ content and $C_3A$ has a higher heat of hydration than the other clinker phases [10], it releases more heat during hydration than Cement 2.

## Interfacial Zone Microstructure

As mentioned previously, a database of stored cement particle shapes and phase distributions may be used along with the NIST microstructure model to simulate the development of microstructure in an interfacial zone in concrete. Figure 6 shows both the original random

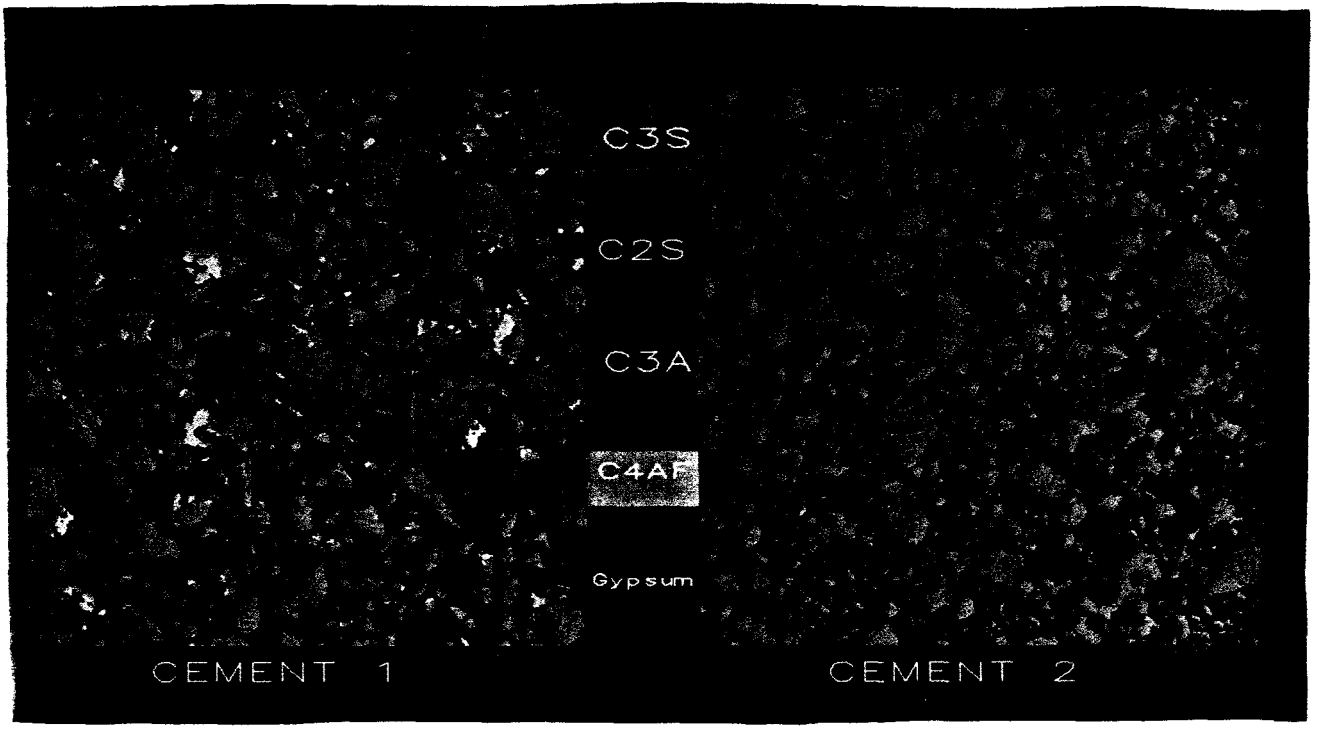


Figure 4. Computer-assembled 250*250 $\mu$m (500*500 pixel) images of initial cement particles for two cements, both with a w/c of 0.45. Color scheme is the same as in Figure 3. Cement 1 contains a higher fraction of $C_3A$ (bright green) than Cement 2.

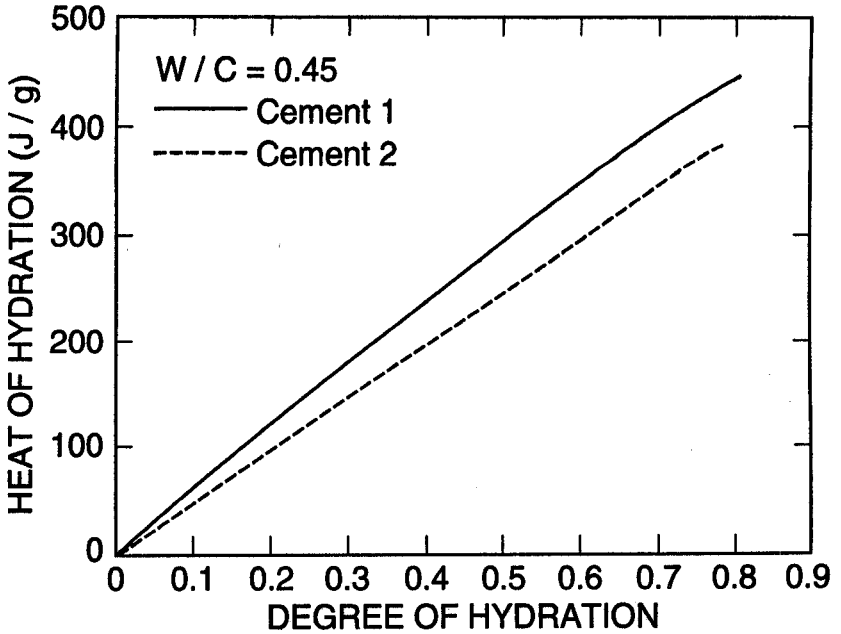


Figure 5. Heat of hydration curves calculated for the two cements shown in Figure 4.

Table 2
Phase Fractions for Cements in Figure 4

| | Cement 1 | | Cement 2 | |
|---|---|---|---|---|
| | Area Fraction | Perimeter Fraction | Area Fraction | Perimeter Fraction |
| $C_3S$ | 0.672 | 0.462 | 0.764 | 0.715 |
| $C_2S$ | 0.118 | 0.307 | 0.110 | 0.101 |
| $C_3A$ | 0.133 | 0.122 | 0.038 | 0.051 |
| $C_4AF$ | 0.038 | 0.020 | 0.00 | 0.00 |
| Gypsum | 0.039 | 0.089 | 0.088 | 0.133 |

configuration of cement particles around an aggregate (purple) for a system with a w/c or 0.45 and the same system after hydration for 150 cycles using the microstructure model. In the hydrated image, C-S-H gel is yellow, CH and iron hydroxide ($FH_3$) are dark and bright blue respectively, and aluminate hydration products (AFt, $C_3AH_6$, etc.) are green. Since the cement particles do not pack efficiently in the vicinity of the aggregate, the interfacial or transition zone contains less cement and more water-filled porosity, thus having a higher local w/c ratio. This local inhomogeneity will affect both the hydration process and the resultant final microstructure.

The hydrated paste microstructure in Figure 6 appears to be different near the aggregate than the bulk paste microstructure far away

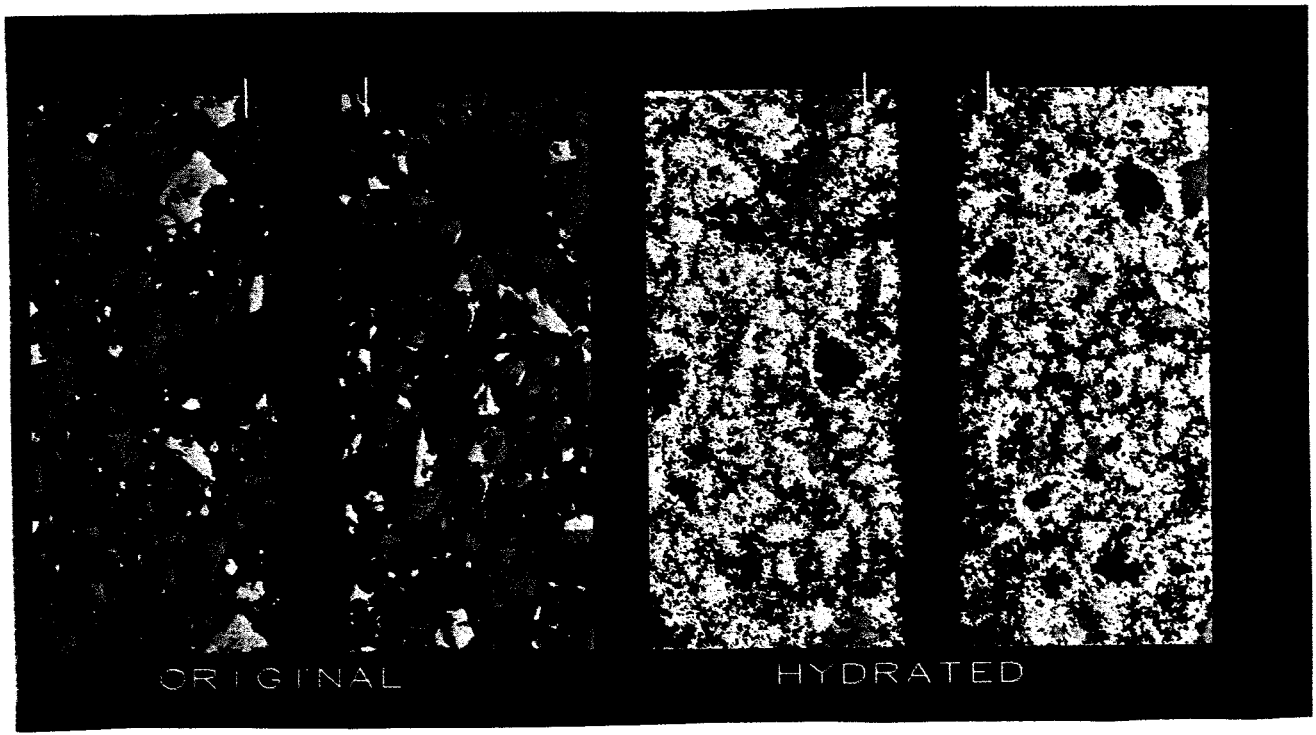


Figure 6. Original and hydrated images showing interfacial zone microstructure. Global w/c is 0.45. White bars at top of images indicate extent (30 pixels) of interfacial zones.

from the aggregate. To quantify this effect, Figure 7 shows a plot of the phase fractions as a function of distance from the aggregate surface for results averaged over five separate configurations of initial microstructures like the one shown in Figure 6. Even after 63% hydration, there is still a large increase in porosity as the aggregate surface is approached. In this region, there is also a deficiency of anhydrous cement, C-S-H, and $FH_3$. Conversely, the more mobile sulfate, calcium, and aluminate species lead to an increase in the CH, AFt, AFm, and $C_3AH_6$ in the area next to the aggregate. Since there is initially more porosity in this area and these mobile species tend to migrate throughout all available porosity, there is ultimately a larger volume of these hydration products formed near the aggregate than in the bulk paste. These computer model results are in agreement with numerous experimental observations [11-15].

## X-ray Images of Hydrated Systems

Because the phase present at each pixel in an image is available as output from the microstructure model, simulated X-ray images can be easily produced. For example, a binary X-ray image for iron could be produced by highlighting all pixels where $C_4AF$ or $FH_3$ is present. To demonstrate this process, Figure 8 shows binary X-ray images for calcium, silicon, iron, and aluminum for both the initial and hydrated interfacial zone model microstructures shown in Figure 6. In each case, the images to the left of the grey aggregate are the initial element distributions. Images on the right are mirror images of the ones on the left, but after 150 cycles of hydration. Here, it is clearly observed that the elements assigned a higher mobility in the model such as calcium and aluminum are indeed dispersed throughout the microstructure

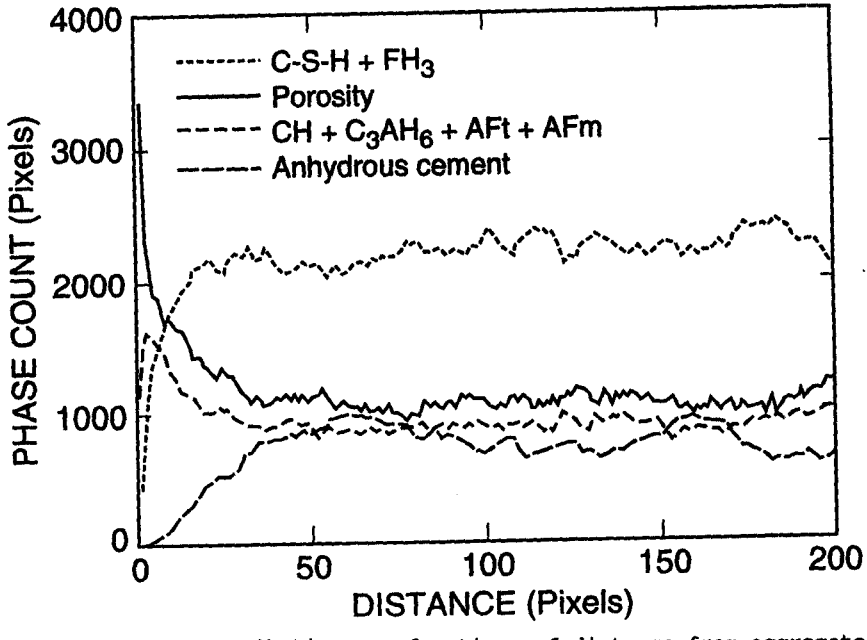


Figure 7. Phase distributions as functions of distance from aggregate surface for hydrated interfacial zone microstructure shown in Figure 6.

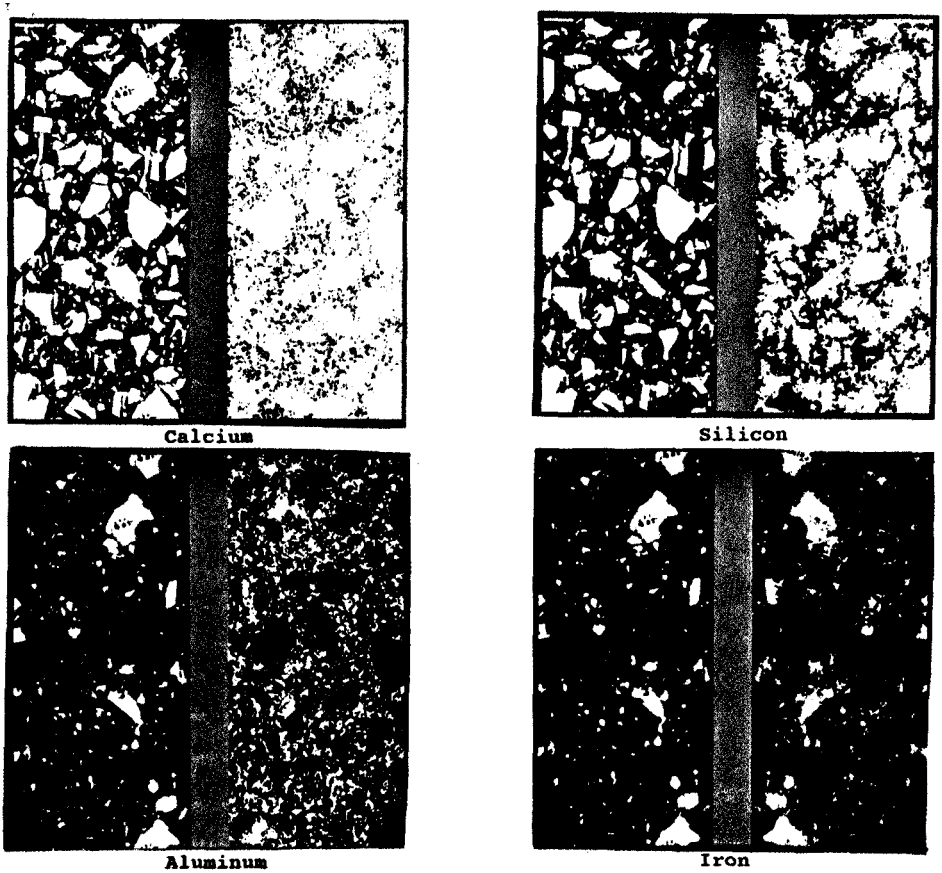


Figure 8. X-ray images for simulated interfacial zone microstructures from Figure 6, before (left) and after (right) 150 cycles (about 28 days) of hydration using the cement microstructure model.

during hydration, while the iron and silicon remain relatively close to their initial locations. These X-ray images could be compared to similar images obtained on real hydrated systems to validate and further improve the microstructure model.

## CONCLUSIONS

A technique for obtaining two-dimensional images of cement particles segmented into individual phases has been demonstrated. The technique allows for quantitative characterization of cement powders, providing information on the distribution of phases not available from typical bulk oxide analyses. The technique can also be used to obtain starting images for cement paste microstructure computer models. The application of these computer models to predicting heat of hydration curves and studying interfacial zone microstructure in concrete has been demonstrated.

**REFERENCES**

[1] Stutzman, P.E., "Cement Clinker Characterization by Scanning Electron Microscopy", Cement, Concrete, and Aggregates, Vol. 13, No. 2, pp. 109-114, 1991.

[2] Scrivener, K.L., "The Microstructure of Anhydrous Cement and Its Effect on Hydration", in Microstructural Development During Hydration of Cement, Materials Research Society Symposia Proceedings Volume 85, Eds. L.J. Struble and P.W. Brown, pp. 39-46, 1987.

[3] Bonen, D., and Diamond, S., "Application of Image Analysis to a Comparison of Ball Mill and High Pressure Roller Mill Ground Cement", in Proceedings of the Thirteenth International Conference on Cement Microscopy, International Cement Microscopy Association, pp. 101-119, 1991.

[4] Bentz, D.P., and Garboczi, E.J., "Digital-Image-Based Computer Modelling of Cement-Based Materials", in Digital Image Processing: Techniques and Applications in Civil Engineering, Engineering Foundation Conference Proceedings, March 1993.

[5] Garboczi, E.J., and Bentz, D.P., "Computational Materials Science of Cement-Based Materials", MRS Bulletin, Vol. 18 (3), pp. 50-54, 1993.

[6] Castleman, K.R., Digital Image Processing, Prentice-Hall, Inc., Englewood Cliffs, NJ, 1979.

[7] Hagwood, C., "A Mathematical Treatment of The Spherical Stereology", NISTIR 4370, U.S. Department of Commerce, 1990.

[8] Bentz, D.P., Coveney, P.V., Garboczi, E.J., Kleyn, M.F., and Stutzman, P.E., "Cellular Automaton Simulations of Cement Hydration and Microstructure Development", submitted to Modelling and Simulation in Materials Science and Engineering.

[9] Taylor, H.F.W., Cement Chemistry, Academic Press, London, 1990.

[10] Neville, A.M., and Brooks, J.J., Concrete Technology, Longman Scientific and Technical, Essex, 1990.

[11] Scrivener, K.L., and Gartner, E.M., "Microstructural Gradients in Cement Paste Around Aggregate Particles", in Bonding in Cementitious Composites, Materials Research Society Symposium Proceedings, Eds. S. Mindess and S.P. Shah, pp. 77-85, 1988.

[12] Monteiro, P.J.M., and Mehta, P.K., "Ettringite Formation on the Aggregate-Cement Paste Interface", Cement and Concrete Research, Vol. 15, No. 2, pp. 378-380, 1985.

[13] Monteiro, P.J.M., Gjorv, O.E., and Mehta, P.K., "Effect of Condensed Silica Fume on the Steel-Cement Paste Transition Zone", Cement and Concrete Research, Vol. 19, No. 1, pp. 114-123, 1989.

[14] Bentz, D.P., Garboczi, E.J., and Stutzman, P.E., "Computer Modelling of the Interfacial Zone in Concrete", RILEM Proceedings Interfaces in Cementitious Composites, Ed. J.C. Maso, Vol. 18, pp. 107-116, 1992.

[15] Maso, J.C., "The Bond Between Aggregates and Hydrated Cement Pastes", Proceedings 7th International Cement Congress, pp. 3-15, 1980.